

Taylor's chiral microswimmer

Harsh Soni 

*Department of Physics, Indian Institute of Science, Bangalore 560 012, India
and School of Physical Sciences, IIT Mandi, Kamand, Mandi, HP 175005, India*



(Received 13 December 2022; accepted 12 April 2023; published 28 April 2023)

In order to understand the rotational motion of a microswimmer in a Newtonian fluid, we model it as an infinite cylinder with a helical, propagating surface wave. Using the method of series expansion, we calculate the linear and angular velocities of the cylinder, assuming that the wave amplitude is much smaller than the wavelength. To the first order in the wave amplitude, for the first mode of a purely azimuthal wave (that is, when the wavelength equals the cylinder's circumference), the cylinder moves along a circular path in the plane normal to its axis. Otherwise, the first-order velocities of the cylinder are zero, like the Taylor sheet. The time-averaged motion of the cylinder is determined by calculating the second-order velocities; the axial component of the wave vector leads to the linear motion of the cylinder along its axis and the azimuthal component to the angular motion around the axis. With the same stroke, the cylinder is always slower and less efficient than the Taylor sheet.

DOI: [10.1103/PhysRevFluids.8.044201](https://doi.org/10.1103/PhysRevFluids.8.044201)

I. INTRODUCTION

Microswimmers swim through a fluid by periodically deforming their bodies in such a way that the time reversal symmetry is broken. Their dynamics happen in a low Reynolds number regime where the inertial effects do not play a significant role: their motility is mainly due to the viscous effects [1]. The swimming mechanism of microswimmers is now well understood; starting from Taylor's sheet, many models have been developed to comprehend various aspects of the dynamics of microswimmers [2–6]. Moreover, there has been considerable research done on how microswimmers interact with each other and with the wall [7–14]. Recently growing understanding of complex fluids has led to increased interest in how fluid complexity impacts the swimming speed [15–23].

So far microswimmers have been studied largely in context of their translational motion. However, the microswimmers such as *Escherichia coli* do not simply propel through the fluid, they also spin around their directions of propulsion [24–27]. Inspired by them we construct a simple model which can explain not only the linear but also the angular motion of microswimmers. On symmetry grounds, one anticipates that a swimmer cannot perform rotational dynamics without having handedness in its structure and inherent movements. So the chirality of the microswimmer is crucial to its angular motion. The helical cylinder, a microswimmer model with chirality, has already been investigated in the context of the linear motion of microorganisms having helical flagella [3,28,29].

Here the microswimmer is modeled as an infinite cylinder whose surface is subject to a prescribed helical wave. The helicity of the wave provides the chirality to the cylinder, which is essential for the rotational motion of microorganisms. The traveling helical wave of cilia movements has been observed on the surface of *Paramecium* [27]. Our calculation relies on the following two assumptions: (1) Reynolds number is zero and (2) the wavelength is much larger than the wave amplitude so that one can expand the velocity and pressure fields in terms of the amplitude. The

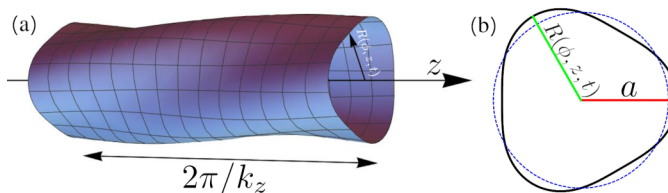


FIG. 1. (a) Schematic diagram of a cylinder whose surface is subject to a helical, propagating wave. The radial coordinate of a surface point on the cylinder at (ϕ, z) is given by $R(\phi, z, t) = a + b \sin(m\phi + k_z z - \omega t)$. (b) The black curve shows the cross section of the cylinder at $z = 0$. Here $m = 3$, $ak_z = 1$, and $b = 0.1a$.

main findings of this paper are as follows: the azimuthal component of the wave vector of the wave is responsible for the angular motion of the cylinder and the axial component for the translational motion. For the first mode of a purely azimuthal wave (i.e., when the wavelength is equal to the circumference of the cylinder), the cylinder performs an orbital motion in the plane normal to its axis, apart from the angular motion. The Taylor sheet is always faster and more efficient than the cylinder for given wavelength, frequency, and amplitude of the wave.

The rest of the paper is organized as follows: Sec. II discusses our model. In Sec. III the results are presented. A brief discussion is provided in Sec. IV. In Sec. V we conclude.

II. MODEL

We consider an infinitely long cylinder of radius a submerged in a Newtonian fluid whose surface is subject to a helical, propagating sinusoidal wave. The reader should note that the centerline of the cylinder remains straight, only the surface deforms, unlike the models presented in [3,28] (see Fig. 5). Let the axis of the cylinder be along the z axis; at time t , the axial distance of a point on the deforming surface having azimuth ϕ and axial position z is given by

$$R(\phi, z, t) = a + b \sin(m\phi + k_z z - \omega t), \quad (1)$$

where m is an integer, $k_z (\geq 0)$ is the z component of the wave vector, and ω and b are the angular frequency and the amplitude of the helical wave, respectively (see Fig. 1). When $m = 1$, our model exhibits some similarities with the model presented by Taylor [3] for helical flagella, but they are not exactly identical (see Appendix A). As the azimuthal component of wave vector is m/a , the “effective” wave number and speed of the helical wave are given by $k = \sqrt{k_z^2 + (m/a)^2}$ and $c = \omega/k$, respectively. We assume that $\epsilon = bk \ll 1$. In our analysis, we consider that $m \geq 0$; the final results remain the same as m changes sign, other than reversing the angular velocity of the cylinder.

A. Equations of motion for the Newtonian fluid

Considering that the fluid is incompressible, the stress tensor for the velocity field \mathbf{u} is given by [30]

$$\boldsymbol{\sigma} = \eta(\nabla \mathbf{u} + \nabla \mathbf{u}^T) - p, \quad (2)$$

where p is the pressure field and η is the dynamic viscosity: the superscript T stands for the matrix transpose. Here the first term is the stress due the viscosity of the fluid. At zero Reynolds number, the fluid is in mechanical equilibrium, i.e., the net force per unit volume on the fluid is zero [30]:

$$\nabla \cdot \boldsymbol{\sigma} = 0. \quad (3)$$

The incompressibility of the fluid leads to the condition

$$\nabla \cdot \mathbf{u} = 0. \quad (4)$$

Substituting σ into Eq. (3) yields

$$\eta \nabla^2 \mathbf{u} - \nabla p = 0. \quad (5)$$

B. Boundary conditions

We solve Eq. (5) in a cylindrical coordinate frame comoving and corotating with the cylinder. Adopting no-slip boundary conditions on the cylinder, the fluid velocity at a surface point $\mathbf{r}_s = R(\phi, z, t)\hat{\rho} + z\hat{z}$ of the cylinder is simply given by the velocity of the surface point $d\mathbf{r}_s/dt$. Thus,

$$\mathbf{u}(\rho = R, \phi, z) = \frac{d\mathbf{r}_s}{dt} = -c\epsilon \cos(m\phi + k_z z - \omega t)\hat{\rho}. \quad (6)$$

Let $-U_m\hat{z}$ and $-\Omega_m\hat{z}$ be the time-averaged linear and angular velocities of the cylinder in the laboratory frame. Then, in the frame attached with the cylinder,

$$\langle u_\phi \rangle|_{\rho \rightarrow \infty} = \rho \Omega_m, \quad (7a)$$

$$\langle u_z \rangle|_{\rho \rightarrow \infty} = U_m, \quad (7b)$$

where the angular bracket stands for the average over time.

As the external force and torque on the cylinder are zero, in the stationary state, the net force and the net torque \mathbf{F} and $\boldsymbol{\tau}$ acting on it due to the fluid should be zero. The formulas to calculate \mathbf{F} and $\boldsymbol{\tau}$ are given in Appendix B 3.

C. Series expansion method for solving the fluid equations

In order to solve the equations discussed above, expanding \mathbf{u} and p in ϵ :

$$\mathbf{u} = \epsilon \mathbf{u}^{(1)} + \epsilon^2 \mathbf{u}^{(2)} + \dots, \quad (8a)$$

$$p = \epsilon p^{(1)} + \epsilon^2 p^{(2)} + \dots. \quad (8b)$$

The two leading-order terms of the boundary condition (6) in ϵ then yield

$$\mathbf{u}^{(1)}(\rho = a) = -c \cos(m\phi + k_z z - \omega t)\hat{\rho}, \quad (9)$$

$$\mathbf{u}^{(2)}(\rho = a) = -\frac{1}{k} \frac{\partial \mathbf{u}^{(1)}}{\partial \rho} \Big|_a \sin(m\phi + k_z z - \omega t). \quad (10)$$

We expand Eq. (5) in ϵ and solve it for $\mathbf{u}^{(1)}$ and $\mathbf{u}^{(2)}$ with the above boundary conditions.

For the case of $m = 1$ and $k_z \neq 0$, the first-order torque normal to the cylinder's axis is found to be nonzero. Its consequences are discussed in Sec. III A. For all other cases, the zero-force and the zero-torque conditions are satisfied.

From the form of the surface wave on the cylinder [see Eq. (1)], one can see that a phase shift of π is equivalent to the transformation $\epsilon \rightarrow -\epsilon$. Since a phase shift alone cannot affect the time-averaged swimming dynamics of the cylinder, one expects U_m and Ω_m to be the even functions of ϵ . Therefore, the leading-order terms of U_m and Ω_m would be quadratic in ϵ . Also, in Eq. (5), η can be absorbed into the pressure p . It is therefore obvious that U_m and Ω_m are independent of η [1].

III. RESULTS

First, we present the dynamics of the cylinder at the first order in ϵ in Sec. III A. We then talk about the second-order results in Sec. III B.

A. The first-order results

Solving Eq. (5) for $\mathbf{u}^{(1)}$, we obtain (see Appendix B 4)

$$u_\rho^{(1)} = u_\rho^{(10)}(\rho) \cos(m\phi + k_z z - \omega t), \quad (11a)$$

$$u_\phi^{(1)} = u_\phi^{(10)}(\rho) \sin(m\phi + k_z z - \omega t), \quad (11b)$$

$$u_z^{(1)} = u_z^{(10)}(\rho) \sin(m\phi + k_z z - \omega t), \quad (11c)$$

where

$$u_\rho^{(10)} = c \left(\frac{a_s \{ [(k_z \rho)^2 - m(m+2)] K_m(k_z \rho) + 2(m+1) k_z \rho K_{m+1}(k_z \rho) \} K_{m+1}(a_s) K_m(a_s)}{k_z \rho \mathcal{F}_m(a_s)} + \frac{a_s^2 [m K_m(k_z \rho) - k_z \rho K_{m+1}(k_z \rho)] K_{m+1}(a_s)^2 - m k_z \rho [k_z \rho K_m(k_z \rho) + (m+2) K_{m+1}(k_z \rho)] K_m(a_s)^2}{k_z \rho \mathcal{F}_m(a_s)} \right), \quad (12a)$$

$$u_\phi^{(10)} = c \frac{m[(m+2) K_m(a_s) - a_s K_{m+1}(a_s)] [a_s K_m(k_z \rho) K_{m+1}(a_s) - k_z \rho K_{m+1}(k_z \rho) K_m(a_s)]}{k_z \rho \mathcal{F}_m(a_s)}, \quad (12b)$$

$$u_z^{(10)} = c \frac{[m K_m(a_s) - a_s K_{m+1}(a_s)] [a_s K_m(k_z \rho) K_{m+1}(a_s) - k_z \rho K_{m+1}(k_z \rho) K_m(a_s)]}{\mathcal{F}_m(a_s)}, \quad (12c)$$

and

$$\begin{aligned} \mathcal{F}_m(a_s) = & [2m(m+2) - a_s^2] K_{m+1}(a_s) K_m(a_s)^2 + a_s^2 K_{m+1}(a_s)^3 + m a_s K_m(a_s)^3 \\ & - (3m+2) a_s K_{m+1}(a_s)^2 K_m(a_s), \end{aligned} \quad (13)$$

with $a_s = a k_z$. Presenting the $k_z = 0$ case first: for $m = 0$ and $k_z = 0$, $\mathbf{u}^{(1)} = 0$ as this case represents a cylinder with no surface waves. Setting $k_z = 0$ into the above equations, for $m > 0$, we obtain

$$u_\rho^{(1)} = \frac{c}{2} \left(\frac{a}{\rho} \right)^{m-1} \left[(m-2) \frac{a^2}{\rho^2} - m \right] \cos(m\phi - \omega t), \quad (14)$$

$$u_\phi^{(1)} = \frac{c}{2} (m-2) \left(\frac{a}{\rho} \right)^{m-1} \left[\frac{a^2}{\rho^2} - 1 \right] \sin(m\phi - \omega t), \quad (15)$$

$$u_z^{(1)} = 0. \quad (16)$$

The vanishing z component of the velocity field is due to the absence of the wave propagation along the z direction. For $m = 1$, that is, the wavelength is equal to the circumference of cylinder, in a Cartesian coordinate frame attached to the cylinder, the first-order velocity field far from the cylinder is given by (also see Appendix D)

$$\lim_{\rho \rightarrow \infty} \epsilon \mathbf{T} \cdot \mathbf{u}^{(1)} = -\frac{1}{2} c \epsilon (\cos \omega t, \sin \omega t, 0). \quad (17)$$

So, in the laboratory frame, the first-order velocity of the cylinder $U_1^{(1)} = (c\epsilon/2)(\cos \omega t, \sin \omega t, 0)$ is nonzero, and the cylinder performs an orbital motion in xy plane with the angular frequency ω on a circular path of radius $b/2$ centered at $(0, b/2, 0)$. This is an interesting observation as no model of microswimmers so far has predicted the motion at the first-order in the wave amplitude, although the time average of the velocity of the cylinder still remains zero. For $m > 1$, $\mathbf{u}^{(1)} \rightarrow 0$ as $\rho \rightarrow \infty$, and hence the first-order velocity of the cylinder is zero.

For $k_z \neq 0$, $\mathbf{u}^{(1)}$ always vanishes at $\rho \rightarrow \infty$. Therefore, the cylinder exhibits no motion to the first order. Figure 2 shows the profile of $\mathbf{u}^{(1)}$ around the cylinder in xy and xz planes for $m = 3$ and $a_s = 1$ at $t = 0$; the vector plot displays the in-plane direction of $\mathbf{u}^{(1)}/c$ and the density plot depicts the value of $u^{(1)}/c$. Clearly, the magnitude $u^{(1)}$ decays to zero with distance from the cylinder.

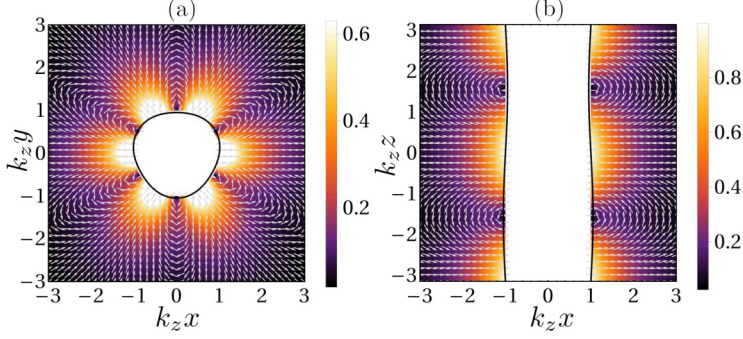


FIG. 2. The first-order velocity field $\mathbf{u}^{(1)}$ around a deforming cylinder shown in Fig. (1) for $k_z \neq 0$. (a) In the xy plane; (b) in the xz plane. The arrow points along the in-plane projection of the direction of $\mathbf{u}^{(1)}$, and the color map displays the magnitude of $\mathbf{u}^{(1)}/c$, where $c \equiv \omega/k$ and $k = \sqrt{k_z^2 + m^2/a^2}$. The black curves represent the cross sections of the surface of the cylinder. Here $m = 3$, $a_s \equiv ak_z = 1$, $b = 0.05a$, and $t = 0$.

Let us now discuss the force and the torque on the cylinder due to the fluid. The first-order force on the cylinder is always zero, but the first-order torque $\boldsymbol{\tau}_1$ turns out to be nonzero when $m = 1$ and $k_z \neq 0$,

$$\boldsymbol{\tau}_1 = \lim_{L_n \rightarrow \infty} \boldsymbol{\tau}_1 \mathbf{n}_\tau, \quad (18)$$

where

$$\mathbf{n}_\tau = \cos(\omega t) \hat{\mathbf{x}} + \sin(\omega t) \hat{\mathbf{y}}, \quad (19)$$

$$\tau_1 = \frac{2\pi L_n (-1)^n \eta \omega a^2 K_1(a_s)^2 K_2(a_s)}{[(a_s^2 + 2)K_1(a_s)^2 K_0(a_s) - a_s^2 K_0(a_s)^3 - a_s K_1(a_s) K_0(a_s)^2 + a_s K_1(a_s)^3] \sqrt{1 + (m/a_s)^2}} \epsilon, \quad (20)$$

and $L_n = 2\pi n/k_z$ is the length of the cylinder between $z = -n\pi/k_z$ and $z = n\pi/k_z$ (see Appendix B 4). Note that the torque $\boldsymbol{\tau}_1$ is periodic with the angular frequency ω . Hence the torque along the cylinder's axis is zero but not normal to it. Here the axis of the cylinder is fixed along the z axis of the laboratory frame; if one allows its rotation, a torque-free cylinder is obtained in the stationary state as $\boldsymbol{\tau}_1$ cancels out with the drag torque $\boldsymbol{\tau}_v$ due to the rotation of the cylinder's axis. For the rotating cylinder, the torque $\boldsymbol{\tau}_1$ would be

$$\boldsymbol{\tau}_1 = \lim_{L_n \rightarrow \infty} \tau_1 [\cos(\omega t) \hat{\mathbf{x}}'(t) + \sin(\omega t) \hat{\mathbf{y}}'(t)] \equiv \lim_{L_n \rightarrow \infty} \tau_1 \mathbf{n}'_\tau, \quad (21)$$

where $\hat{\mathbf{x}}'$ and $\hat{\mathbf{y}}'$ corotate with the cylinder. Let $\Psi_{\text{rot}}^{(1)}$ be the angular speed of the cylinder around \mathbf{n}'_τ . Then [31,32]

$$\boldsymbol{\tau}_v \simeq - \lim_{L_n \rightarrow \infty} \frac{\pi \eta L_n^3}{3 \ln(L_n/a)} \Omega_{\text{rot}}^{(1)} \mathbf{n}'_\tau. \quad (22)$$

The ϵ -dependent corrections have been neglected here. In the stationary state, $\boldsymbol{\tau}_v + \boldsymbol{\tau}_1 = 0$, thus

$$\Omega_{\text{rot}}^{(1)} = \lim_{L_n \rightarrow \infty} \frac{3\tau_1 \ln(L_n/a)}{\pi \eta L_n^3}. \quad (23)$$

From Eq. (20), $\Omega_{\text{rot}}^{(1)} \rightarrow 0$. Therefore, the torque $\boldsymbol{\tau}_1$ tries to rotate the cylinder, but the drag torque $\boldsymbol{\tau}_v$ suppresses the rotation in the $L_n \rightarrow \infty$ limit. However, the actual microorganisms have a finite length and therefore their axes should exhibit a periodic rotational dynamics due to the torque $\boldsymbol{\tau}_1$.

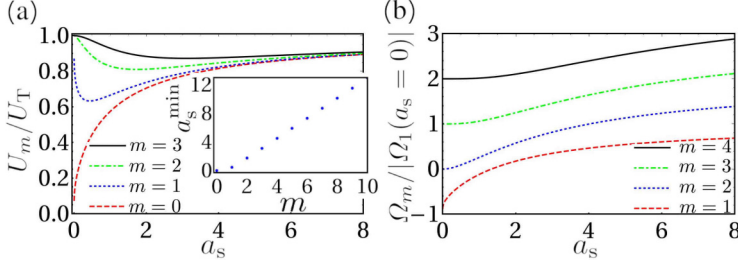


FIG. 3. The components of the linear and angular velocities of the cylinder along the $-\hat{z}$ direction, U_m and Ω_m as the function of a_s for various values of m . (a) U_m/U_T vs a_s , where U_T is the speed of the Taylor sheet with the wave number k_z . The inset shows how the location of the minimum of U_m depends on m . (b) $\Omega_m/|\Psi_1(a_s = 0)|$ vs a_s .

B. The second-order results

To calculate the time-averaged translational and angular speeds of the cylinder, we solve Eq. (5) for $\langle \mathbf{u}^{(2)} \rangle$, which yields (see Appendix B 5)

$$\langle u_\rho^{(2)} \rangle = 0, \quad (24a)$$

$$\langle u_\phi^{(2)} \rangle = ck_z \rho \frac{[a_s K_{m-1}(a_s) + m K_m(a_s)] \mathcal{G}_m(a_s)}{2 \mathcal{F}_m(a_s) \sqrt{(1 + m^2/a_s^2)}}, \quad (24b)$$

$$\langle u_z^{(2)} \rangle = c \frac{m[(2 - m)K_m(a_s) - a_s K_{m-1}(a_s)] \mathcal{G}_m(a_s)}{2 a_s^2 \mathcal{F}_m(a_s) \sqrt{(1 + m^2/a_s^2)}}, \quad (24c)$$

where $\mathcal{G}_m(a_s) = a_s(K_{m-1}(a_s)^2 - K_m(a_s)^2) + 2mK_m(a_s)K_{m-1}(a_s)$.

In the $\rho \rightarrow \infty$ limit, $\langle u_\phi^{(2)} \rangle$ is proportional to ρ ; thus the cylinder has a nonzero angular velocity around its axis. From Eqs. (7), the time-averaged components of the angular and the linear velocities of the cylinder along the $-\hat{z}$ direction are

$$\Omega_m \simeq \lim_{\rho \rightarrow \infty} \frac{1}{\rho} \langle u_\phi^{(2)}(\rho) \rangle \epsilon^2 \simeq -ck_z \frac{[a_s K_{m-1}(a_s) + m K_m(a_s)] \mathcal{G}_m(a_s)}{2 \mathcal{F}_m(a_s) \sqrt{(1 + m^2/a_s^2)}} \epsilon^2, \quad (25)$$

$$U_m \simeq \lim_{\rho \rightarrow \infty} \langle u_z^{(2)}(\rho) \rangle \epsilon^2 \simeq c \frac{m[(2 - m)K_m(a_s) - a_s K_{m-1}(a_s)] \mathcal{G}_m(a_s)}{2 a_s^2 \mathcal{F}_m(a_s) \sqrt{(1 + m^2/a_s^2)}} \epsilon^2. \quad (26)$$

If the surface wave is purely axial, namely, $m = 0$, then $\Omega_0 = 0$, as expected because the cylinder loses its chirality, and

$$U_0 = -\frac{1}{2} \left[\frac{a_s [K_0(a_s)^2 - K_1(a_s)^2]}{a_s K_0(a_s)^2 + 2K_1(a_s)K_0(a_s) - a_s K_1(a_s)^2} \right] c \epsilon^2, \quad (27)$$

with $\epsilon = k_z b$ and $c = \omega/k_z$; $U_0 \geq 0$, as seen for the Taylor sheet [2] [see Fig. 3(a)]. In the $a_s \rightarrow \infty$ limit, U_0 approaches $U_T = \omega k_z b^2 / 2$, the speed of the Taylor sheet having the wave number k_z , since a cylinder with an infinitely large radius is just like a flat sheet. For $a_s \ll 1$,

$$U_0 \simeq -\frac{1}{4[\ln(a_s/2) + \gamma]} c \epsilon^2, \quad (28)$$

where $\gamma = 0.5772$ is the Euler-Mascheroni constant; $U_0 \rightarrow 0$ as $a_s \rightarrow 0$.

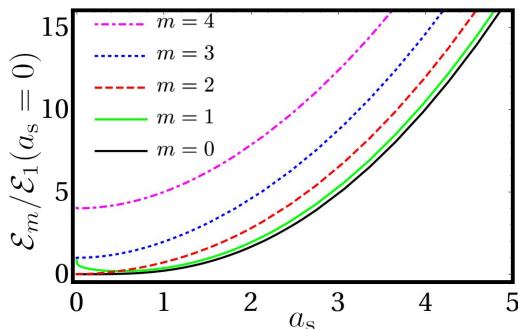


FIG. 4. The efficiency of the cylinder \mathcal{E}_m scaled by its value at $m = 1$ and $a_s = 0$ as the function a_s for $m = 0, 1, 2$, and 3.

When the surface wave is purely azimuthal, that is, $k_z = 0$, the cylinder does not perform any translational motion, namely, $U_m = 0$. In this case, $\Omega_0 = 0$, and

$$\Omega_{m>0}(k_z = 0) = \frac{m-2}{2m^2} \epsilon^2 \omega = \frac{m-2}{2a^2} b^2 \omega. \quad (29)$$

Interestingly, $\Omega_1(k_z = 0) < 0$, i.e., the cylinder spins in the same direction as the direction of the surface wave for $m = 1$. Up to the second order in ϵ , the cylinder with the second mode ($m = 2$) of a purely azimuthal surface wave does not spin because $\Omega_2(k_z = 0) = 0$.

Figure 3(a) illustrates how U_m varies with a_s for various values of m ; U_0/U_T increases monotonically with a_s , whereas for $m \geq 1$, U_m/U_T attains its minimum value at a value a_s^{\min} of a_s . As shown in the inset of Fig. 3(a), a_s^{\min} increases almost linearly with m . In the $a_s \rightarrow 0$ limit, $U_0/U_T \rightarrow 0$ and $U_{m>1}/U_T \rightarrow 1$. In the large a_s limit, $U_m/U_T \simeq 1$, so the cylinder swims with the speed of the Taylor sheet for all m . For given a_s , the swimming speed U_m is enhanced with increasing m . As $U_m \leq U_T$, the cylinder cannot swim faster than the Taylor sheet having the wave number k_z .

Figure 3(b) shows that Ω_m scaled by $|\Omega_1(a_s = 0)|$ grows with a_s for all values of m ; Ω_1 remains negative below $a_s \simeq 1.33$. As $a_s \rightarrow \infty$, $\Omega_m/|\Omega_1(a_s = 0)|$ saturates to m . Again, for given a_s , increasing m boosts the angular speed of the cylinder.

We now estimate the mechanical efficiency of the cylinder. The time-averaged velocity of a surface point of the cylinder at (ϕ, z) is $\mathbf{U}_s = -\Omega_m a \hat{\phi} - U_m \hat{z}$, so the thrust force per area on the cylinder would be proportional to $\eta k |\mathbf{U}_s|$ [5]. Therefore, one can define the mechanical efficiency of the cylinder as follows:

$$\mathcal{E}_m \simeq \eta \frac{|\mathbf{U}_s|^2}{\mathcal{W}^{(0)}} k \simeq \eta \frac{U_m^2 + \Omega_m^2 a^2}{\mathcal{W}^{(0)}} k, \quad (30)$$

where $\mathcal{W}^{(0)}$ is the leading-order term of the rate of the work performed by the cylinder per area on the fluid (see Appendix C). Note that $\mathcal{W}^{(0)} \sim \epsilon^2$. Therefore, $\mathcal{E}_m \sim \epsilon^2$, as $|\mathbf{U}_s| \sim \epsilon^2$. For $k_z = 0$ case: $\mathcal{E}_0 = 0$ and

$$\mathcal{E}_{m>0}(k_z = 0) = \frac{(m-2)^2}{4m^2} \epsilon^2 = \frac{(m-2)^2}{4a^2} b^2, \quad (31)$$

so $\mathcal{E}_2(k_z = 0)$ is also zero. This is because both translational and angular velocities are zero when $m = 2$ and $k_z = 0$. The efficiency \mathcal{E}_m is a monotonically rising function of a_s for all m , excluding the $m = 1$ case; see Fig. 4. For $m = 1$, the magnitude of the angular velocity is minimum at

$a_s = 1.33$, thus \mathcal{E}_1 is not a monotonic function of a_s . In the $a_s \rightarrow \infty$ limit, \mathcal{E}_m achieves its largest value,

$$\mathcal{E}_m(a_s \rightarrow \infty) = \frac{1}{4}b^2k_z^2, \quad (32)$$

which is the same as the efficiency of the Taylor sheet [1] of the wave number k_z . Therefore, the cylinder is always less efficient as compared to the Taylor sheet. One can also see from Fig. 4 that, if the $m = 1$ case ignored, the higher the value of m , the more efficient the cylinder is.

IV. DISCUSSION

It should be noted that the dynamics of the cylinder is anomalous for the $m = 1$ case, for which, to first order in ϵ , the cylinder with $k_z = 0$ displays an orbital motion due to the first-order flow profile, whereas, for $k_z \neq 0$, the first-order torque normal to the axis of the cylinder is nonzero. Moreover, below $a_s \simeq 1.33$, $\Omega_1 < 0$, namely, the cylinder (with $m = 1$) rotates along the direction of the azimuthal projection of the wave vector. It can be understood as follows: time averaging the azimuthal component of Eq. (10) yields

$$\langle u_\phi^{(2)}(\rho = a) \rangle = -\frac{1}{2k} \left. \frac{du_\phi^{(10)}}{d\rho} \right|_a. \quad (33)$$

As $\langle u_\phi^{(2)} \rangle = H_2\rho$ [see Appendix (B 5)],

$$H_2 = -\frac{1}{2ak} \left. \frac{du_\phi^{(10)}}{d\rho} \right|_a. \quad (34)$$

Then, from the condition (7a),

$$\Omega_m = H_2 = -\frac{1}{2ak} \left. \frac{du_\phi^{(10)}}{d\rho} \right|_a. \quad (35)$$

So, mathematically, the angular motion of the cylinder is due to the nonzero value of the derivative of $u_\phi^{(10)}$ at $\rho = a$; for $m > 1$, it is negative, so $\Omega_m > 0$. For $m = 1$, it becomes positive below $a_s = a_s^c$. From Eq. (12b), a_s^c is given by the solution of

$$3K_1(a_s) - a_s K_2(a_s) = 0, \quad (36)$$

that is, $a_s^c \simeq 1.33158$. Hence $\Omega_1 < 0$ for $a_s < a_s^c \simeq 1.33158$. Note that $u_\phi^{(10)} = 0$ at $a_s = a_s^c$.

As mentioned earlier, the microswimmer models with chirality have already been explored [3,28], although with the goal to understand the translational motion. Taylor [3] considered a cylinder in a Newtonian fluid whose centerline is subject to a spiral propagating wave. When the wave amplitude is much smaller than the radius of the cylinder, the shape of the Taylor cylinder is similar to that of our cylinder with $m = 1$ (see Appendix A). A subtle difference between the two models appears at the level of the surface dynamics; in our model, the velocity of a surface point has no azimuthal component, unlike the Taylor model. Taylor saw an increment in the translational speed due to the chirality, and the same trend is observed here as well: one can see from Fig. 3 that the speed $U_{m>0}$ of chiral cylinders is always greater than the speed U_0 of the achiral cylinder.

The Taylor model is appropriate for the microorganisms having helical flagella, e.g., *E. coli*, whereas our model is suitable for ciliated microorganisms with metachronal waves, e.g., *Pleurobrachia*, *Opalina*, and *Paramecium* [33]. The typical values of m and k_z for *Paramecia* are 4–8 and 10^5 m^{-1} , respectively [34,35]. This paper primarily focuses on chiral microswimmers, but we also investigate the special case of our model with no chirality, namely, the $m = 0$

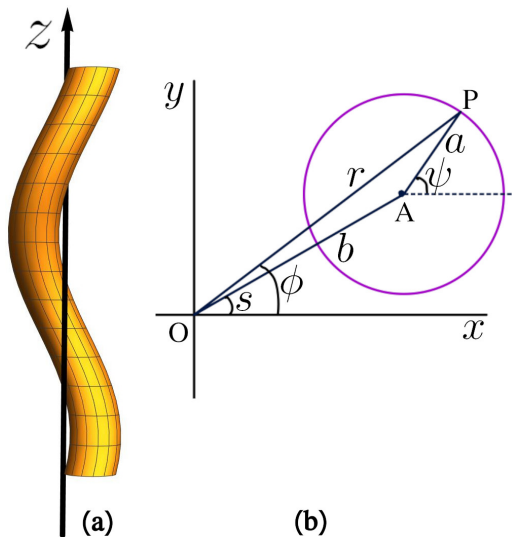


FIG. 5. (a) Schematic diagram of the spiral cylinder modeled by Taylor [3]. In contrast to our model, the centerline of the cylinder is not straight here. (b) Cross section of the cylinder in the xy plane. Here $s = -k_z z + \omega t$, a is the radius of the cylinder, and b represents the radial coordinate of its center A. The position of a surface point P in terms of ψ and z is given by $\mathbf{R} = a(\cos \psi \hat{\mathbf{x}} + \sin \psi \hat{\mathbf{y}}) + b(\cos s \hat{\mathbf{x}} + \sin s \hat{\mathbf{y}}) + z \hat{\mathbf{z}}$. Note that $b \ll a$, although the figure does not reflect so.

case; metachronal waves of *Pleurobrachia* and *Opalina* are not helical and thus belong to this case.

V. CONCLUSION

We calculated the linear and angular velocities of an infinite cylinder with a propagating, helical surface wave in a Newtonian fluid. Assuming that the amplitude b of the wave is much smaller than its wavelength λ , we use the series expansion method to solve the Stokes equations for the fluid. To the first order in $\epsilon \equiv 2\pi b/\lambda$, the cylinder with the first mode of a purely azimuthal wave (i.e., $m = 1$ case) exhibits an orbital motion on a circular path normal to its axis. To the second order in ϵ , the azimuthal component of the wave vector gives rise to the angular dynamics, whereas the axial component does to the translational dynamics. With the same wave, the Taylor sheet is always faster and more efficient than the cylinder.

APPENDIX A: TAYLOR'S MODEL FOR HELICAL FLAGELLA

Here we provide a brief discussion of the model presented by Taylor [3] that explains the swimming dynamics of helical flagella. He considered a cylinder whose centerline is subject to a spiral wave, as illustrated in Fig. 5(a). In terms of the angle ψ shown in Fig. 5(b), the position of a surface point P on the cylinder is given by

$$\mathbf{R} = a(\cos \psi \hat{\mathbf{x}} + \sin \psi \hat{\mathbf{y}}) + b(\cos s \hat{\mathbf{x}} + \sin s \hat{\mathbf{y}}) + z \hat{\mathbf{z}}, \quad (\text{A1})$$

where $s = -k_z z + \omega t$ is the angular coordinate of the center A of the cylinder, which varies with time t as well as z . So, for given z , the center of cylinder moves on a circular path of radius b . In the $b \ll a$ limit, the radial coordinate of P in terms of its angular coordinate ϕ is given by

$$r \simeq a + b \cos(\phi - s) \simeq a + b \cos(\phi + k_z z - \omega t). \quad (\text{A2})$$

As the cylinder deforms with time, ϕ also changes due to the motion of its centerline. It implies that the azimuthal component of the velocity of the surface point P is nonzero. A simple calculation gives the following approximate velocity of P (in the frame moving with the cylinder):

$$\mathbf{V} \simeq \omega b \sin(\phi - s) \hat{\rho} + \omega b \cos(\phi - s) \hat{\phi}. \quad (\text{A3})$$

It should be noted that, with respect to its shape, the model being discussed exhibits similarities to our model with $m = 1$ [see Eqs. (1) and (A2)]. However, unlike our model, the azimuthal component of the surface velocity is nonzero. As previously mentioned, this is due to the dynamics of the cylinder's centerline.

APPENDIX B: SOLUTION OF THE EQUATIONS OF MOTION FOR THE FLUID

1. Equations of motion for the fluid

Recalling equations of motion for the Newtonian fluid [see Eq. (5)],

$$\eta \nabla^2 \mathbf{u} - \nabla p = 0, \quad (\text{B1})$$

where p and \mathbf{u} are the pressure and the velocity fields of the fluid, respectively. In order to eliminate p , we take the curl of the above equation. This yields

$$\nabla^2 \boldsymbol{\Omega} = 0, \quad (\text{B2})$$

where

$$\boldsymbol{\Omega} = \nabla \times \mathbf{u} \quad (\text{B3})$$

is the vorticity. Recalling the incompressibility condition (4),

$$\nabla \cdot \mathbf{u} = 0. \quad (\text{B4})$$

2. Model

Consider an infinite cylinder of radius a in the fluid along the z axis whose surface is subject to a propagating, helical wave of deformation. The radial coordinate of a surface point on the cylinder at (ϕ, z) , at time t , is given by $R(\phi, z, t) = a + b \sin(m\phi + k_z z - \omega t)$, where m is a positive integer, k_z is the z component of the wave vector, and ω and b are the angular frequency and the amplitude of the wave, respectively. For simplicity, the units of length and time are chosen to be $1/k_z$ and $1/\omega$, respectively. Then

$$R(\phi, z, t) = a_s + \epsilon \frac{1}{\sqrt{1 + (m/a_s)^2}} \sin(m\phi + z - t), \quad (\text{B5})$$

where $a_s = ak_z$, $k = \sqrt{k_z^2 + (m/a)^2}$ and $\epsilon = bk$; k is the effective wave number of the wave. Assuming that $\epsilon \ll 1$. We solve Eq. (B2) in a cylindrical coordinate system comoving and corotating with the cylinder. We consider no-slip boundary condition at the surface of the cylinder; then the velocity of the fluid at a surface point $\mathbf{r}_s = R(\phi, z, t) \hat{\rho} + z \hat{\mathbf{z}}$ of the cylinder is equal to the velocity of the surface point. So

$$\mathbf{u}(\rho = R, \phi, z) = \frac{d\mathbf{r}_s}{dt} = -\epsilon \frac{1}{\sqrt{1 + (m/a_s)^2}} \cos(m\phi + z - t) \hat{\rho}. \quad (\text{B6})$$

As we are interested in $\epsilon \ll 1$ regime, we can expand \mathbf{u} and p in ϵ as follows:

$$\mathbf{u} = \epsilon \mathbf{u}^{(1)} + \epsilon^2 \mathbf{u}^{(2)} + \dots, \quad (\text{B7a})$$

$$p = \epsilon p^{(1)} + \epsilon^2 p^{(2)} + \dots. \quad (\text{B7b})$$

The ϵ and ϵ^2 terms of Eq. (B6) yield

$$\mathbf{u}^{(1)}(\rho = a_s) = -\frac{1}{\sqrt{1 + (m/a_s)^2}} \cos(m\phi + z - t) \hat{\rho}, \quad (\text{B8})$$

$$\mathbf{u}^{(2)}(\rho = a_s) = -\frac{1}{\sqrt{1 + (m/a_s)^2}} \left. \frac{\partial \mathbf{u}^{(1)}}{\partial \rho} \right|_{a_s} \sin(m\phi + z - t). \quad (\text{B9})$$

Equation (B2) is now expanded in ϵ and solved for $\mathbf{u}^{(1)}$ and $\mathbf{u}^{(2)}$ with the above boundary conditions.

3. The force and the torque exerted by the fluid on the cylinder

The force \mathbf{F} and the torque $\boldsymbol{\tau}$ on the cylinder in a Cartesian coordinate system are given by

$$\mathbf{F} = \iint \mathbf{T} \cdot \boldsymbol{\sigma}_s \cdot d\mathbf{A} = \lim_{n \rightarrow \infty} \int_0^{2\pi} d\phi \int_{-n\pi/k_z}^{n\pi/k_z} dz \mathbf{T} \cdot \boldsymbol{\sigma}_s \cdot \hat{\mathbf{n}} \text{Det}[\mathbf{g}]^{1/2} \quad (\text{B10})$$

and

$$\boldsymbol{\tau} = \iint \mathbf{T} \cdot [\mathbf{r}_s \times \boldsymbol{\sigma}_s \cdot d\mathbf{A}] = \lim_{n \rightarrow \infty} \int_0^{2\pi} d\phi \int_{-n\pi/k_z}^{n\pi/k_z} dz \mathbf{T} \cdot [\mathbf{r}_s \times \boldsymbol{\sigma}_s \cdot \hat{\mathbf{n}}] \text{Det}[\mathbf{g}]^{1/2}, \quad (\text{B11})$$

where n is a positive integer, $\boldsymbol{\sigma}_s \equiv \boldsymbol{\sigma}(R, \phi, z)$ [see Eq. (2)],

$$\hat{\mathbf{n}}(\phi, z) = \left[\frac{1}{|\nabla[\rho - R(\phi, z, t)]|} \nabla[\rho - R(\phi, z, t)] \right]_{\rho=R} \quad (\text{B12})$$

is the direction of a surface element,

$$\mathbf{g} = \begin{bmatrix} \frac{\partial \mathbf{r}_s}{\partial \phi} \cdot \frac{\partial \mathbf{r}_s}{\partial \phi} & \frac{\partial \mathbf{r}_s}{\partial \phi} \cdot \frac{\partial \mathbf{r}_s}{\partial z} & \frac{\partial \mathbf{r}_s}{\partial z} \cdot \frac{\partial \mathbf{r}_s}{\partial \phi} \\ \frac{\partial \mathbf{r}_s}{\partial \phi} \cdot \frac{\partial \mathbf{r}_s}{\partial z} & \frac{\partial \mathbf{r}_s}{\partial z} \cdot \frac{\partial \mathbf{r}_s}{\partial z} & \frac{\partial \mathbf{r}_s}{\partial z} \cdot \frac{\partial \mathbf{r}_s}{\partial \phi} \\ \frac{\partial \mathbf{r}_s}{\partial z} \cdot \frac{\partial \mathbf{r}_s}{\partial \phi} & \frac{\partial \mathbf{r}_s}{\partial z} \cdot \frac{\partial \mathbf{r}_s}{\partial z} & \frac{\partial \mathbf{r}_s}{\partial \phi} \cdot \frac{\partial \mathbf{r}_s}{\partial z} \end{bmatrix} \quad (\text{B13})$$

is the metric tensor for the surface and

$$\mathbf{T} = \begin{bmatrix} \cos \phi & -\sin \phi & 0 \\ \sin \phi & \cos \phi & 0 \\ 0 & 0 & 1 \end{bmatrix} \quad (\text{B14})$$

is the transformation matrix from the cylindrical to the Cartesian coordinate system at (ϕ, z) .

4. The first-order solution

From the boundary condition (B8) and the incompressibility condition (B4) in the cylindrical coordinate system,

$$\frac{1}{\rho} \frac{\partial(\rho u_\rho)}{\partial \rho} + \frac{1}{\rho} \frac{\partial u_\phi}{\partial \phi} + \frac{\partial u_z}{\partial z} = 0, \quad (\text{B15})$$

we expect the following form of $\mathbf{u}^{(1)}$:

$$u_\rho^{(1)} = u_\rho^{(10)}(\rho) \cos(m\phi + z - t), \quad (\text{B16a})$$

$$u_\phi^{(1)} = u_\phi^{(10)}(\rho) \sin(m\phi + z - t), \quad (\text{B16b})$$

$$u_z^{(1)} = u_z^{(10)}(\rho) \sin(m\phi + z - t). \quad (\text{B16c})$$

Then, solving Eq. (B2) for $u_\rho^{(10)}$, $u_\phi^{(10)}$, and $u_z^{(10)}$, we get

$$u_\rho^{(10)} = \frac{1}{2}(-A_1 + B_1 + 2D_1)K_{m+1}(\rho) - \frac{1}{4\rho}\{A_1(m^2 + \rho^2) - B_1[(m-4)m + \rho^2] + 4D_1m\}K_m(\rho), \quad (\text{B17a})$$

$$u_\phi^{(10)} = -\frac{m}{4\rho}[A_1(m+4) - B_1m - 4D_1]K_m(\rho) - \frac{1}{4}[A_1(m+2) - B_1(m-2)]K_{m-1}(\rho), \quad (\text{B17b})$$

$$u_z^{(10)} = \frac{1}{8}\rho(B_1 - A_1)[K_{m+1}(\rho) + K_{m-1}(\rho)] + D_1K_m(\rho), \quad (\text{B17c})$$

where K_m is the modified Bessel functions of order m . We have ignored the terms having the modified Bessel functions of the second kind I_m to avoid the diverging velocity field at $\rho \rightarrow \infty$. We then calculate the constants A_1 , B_1 , and D_1 by imposing the boundary condition (B8). Substituting their values back into Eqs. (B17) yields

$$u_\rho^{(10)} = \frac{a_s^2[mK_m(\rho) - \rho K_{m+1}(\rho)]K_{m+1}(a_s)^2 + a_s\{[\rho^2 - m(m+2)]K_m(\rho) + 2(m+1)\rho K_{m+1}(\rho)\}K_{m+1}(a_s)K_m(a_s)}{\rho\mathcal{F}_m(a_s)\sqrt{1+(m/a_s)^2}} - \frac{m\rho[\rho K_m(\rho) + (m+2)K_{m+1}(\rho)]K_m(a_s)^2}{\rho\mathcal{F}_m(a_s)\sqrt{1+(m/a_s)^2}}, \quad (\text{B18a})$$

$$u_\phi^{(10)} = \frac{m[(m+2)K_m(a_s) - a_s K_{m+1}(a_s)][a_s K_m(\rho)K_{m+1}(a_s) - \rho K_{m+1}(\rho)K_m(a_s)]}{\rho\mathcal{F}_m(a_s)\sqrt{1+(m/a_s)^2}}, \quad (\text{B18b})$$

$$u_z^{(10)} = \frac{[mK_m(a_s) - a_s K_{m+1}(a_s)][a_s K_m(\rho)K_{m+1}(a_s) - \rho K_{m+1}(\rho)K_m(a_s)]}{\mathcal{F}_m(a_s)\sqrt{1+(m/a_s)^2}}, \quad (\text{B18c})$$

where

$$\mathcal{F}_m(a_s) = [2m(m+2) - a_s^2 K_{m+1}(a_s)K_m(a_s)^2 + a_s^2 K_{m+1}(a_s)^3 + ma_s K_m(a_s)^3 - (3m+2)a_s K_{m+1}(a_s)^2 K_m(a_s)]. \quad (\text{B19})$$

Note that here the unit of velocity is ω/k_z , so one needs to multiply the above expressions with ω/k_z to obtain $u_\rho^{(10)}$, $u_\phi^{(10)}$, and $u_z^{(10)}$ in the original units (the units used in the main text).

We now calculate the first-order pressure $p^{(1)}$. Equation (B1) indicates that $p^{(1)}$ has the form $p^{(1)} = p^{(10)}(\rho) \cos(m\phi + z - t)$. The z component of Eq. (B1) then reads

$$p^{(10)} = -\eta\mathcal{L}^m u_z^{(10)}, \quad (\text{B20})$$

where

$$\mathcal{L}^m \equiv \frac{1}{\rho} \frac{\partial}{\partial \rho} \left(\rho \frac{\partial}{\partial \rho} \right) - \frac{m^2}{\rho^2} - 1. \quad (\text{B21})$$

Substitution of (B18c) into the above equation returns

$$p^{(10)} = \frac{2\eta K_m(\rho)K_m(a_s)[a_s K_{m-1}(a_s) + mK_m(a_s)]}{\mathcal{F}_m(a_s)\sqrt{1+(m/a_s)^2}}. \quad (\text{B22})$$

The above expression is multiplied with ω to obtain $p^{(10)}$ in the units used in the main text.

Due to the periodicity of the cylinder, the ϵ terms of the net force and the torque on the cylinder, \mathbf{F}_1 and $\boldsymbol{\tau}_1$, turn out to be zero, except for the case when $m = 1$ and $k \neq 0$; in this case, the force \mathbf{F}_1 is zero but the torque

$$\boldsymbol{\tau}_1 = \lim_{n \rightarrow \infty} \tau_1 [\cos(t)\hat{\mathbf{x}} + \sin(t)\hat{\mathbf{y}}] \quad (\text{B23})$$

is not, where

$$\tau_1 = \frac{4\pi^2 n (-1)^n \eta a_s^2 K_1(a_s)^2 K_2(a_s)}{[(a_s^2 + 2)K_1(a_s)^2 K_0(a_s) - a_s^2 K_0(a_s)^3 - a_s K_1(a_s) K_0(a_s)^2 + a_s K_1(a_s)^3] \sqrt{1 + (m/a_s)^2}} \epsilon. \quad (\text{B24})$$

The above expression is multiplied with ω/k_z^3 to obtain τ_1 in the units used in the main text.

5. The second-order solution

The boundary condition on $\mathbf{u}^{(2)}$ [see Eq. (D4)] and the form of $\mathbf{u}^{(1)}$ [see Eqs. (B16)] imply that $\mathbf{u}^{(2)}$ has the following form:

$$u_\rho^{(2)} = u_\rho^{(20)}(\rho) + u_\rho^{(21)}(\rho) \sin[2(m\phi + z - t)], \quad (\text{B25a})$$

$$u_\phi^{(2)} = u_\phi^{(20)}(\rho) + u_\phi^{(21)}(\rho) \cos[2(m\phi + z - t)], \quad (\text{B25b})$$

$$u_z^{(2)} = u_z^{(20)}(\rho) + u_z^{(21)}(\rho) \cos[2(m\phi + z - t)]. \quad (\text{B25c})$$

We are interested in the flow profile far away from the cylinder. The harmonic terms in $\mathbf{u}^{(2)}$ vanish in the $\rho \rightarrow \infty$ limit, as seen for $\mathbf{u}^{(1)}$. Therefore, in the $\rho \rightarrow \infty$ limit, $\mathbf{u}^{(2)}$ is simply given by its time-averaged value $\langle \mathbf{u}^{(2)} \rangle$. As $\langle \mathbf{u}^{(2)} \rangle$ is independent of ϕ and z , taking the time average of the second-order terms of Eqs. (B2), (B3), and (B4), we find

$$\frac{d}{d\rho} \rho \langle u_\rho^{(2)} \rangle = 0, \quad (\text{B26a})$$

$$\frac{d}{d\rho} \left(\rho \frac{d^2}{d\rho^2} \langle u_z^{(2)} \rangle \right) - \frac{1}{\rho} \frac{d}{d\rho} \langle u_z^{(2)} \rangle = 0, \quad (\text{B26b})$$

$$\rho^3 \frac{d^3}{d\rho^3} \langle u_\phi^{(2)} \rangle + 2\rho^2 \frac{d^2}{d\rho^2} \langle u_\phi^{(2)} \rangle - \rho \frac{d}{d\rho} \langle u_\phi^{(2)} \rangle + \langle u_\phi^{(2)} \rangle = 0. \quad (\text{B26c})$$

The solutions of these equations are

$$\langle u_\rho^{(2)}(\rho) \rangle = \frac{E_1}{\rho}, \quad (\text{B27a})$$

$$\langle u_\phi^{(2)}(\rho) \rangle = \frac{H_1}{\rho} + H_2 \rho + H_3 \rho \ln \rho, \quad (\text{B27b})$$

$$\langle u_z^{(2)}(\rho) \rangle = \frac{G_1 \rho^2}{2} + G_2 \ln \rho + G_3. \quad (\text{B27c})$$

For a cylinder spinning with a constant angular speed around z axis, $\langle u_\phi^{(2)}(\rho) \rangle \propto \rho$ in the $\rho \rightarrow \infty$ limit, so we cannot throw the $H_2 \rho$ term in the expression of $\langle u_\phi^{(2)}(\rho) \rangle$. To avoid the divergence of the velocity field in the laboratory frame, we set H_3 , G_1 , and G_2 to zero:

$$\langle u_\rho^{(2)}(\rho) \rangle = \frac{E_1}{\rho}, \quad (\text{B28a})$$

$$\langle u_\phi^{(2)}(\rho) \rangle = \frac{H_1}{\rho} + H_2 \rho, \quad (\text{B28b})$$

$$\langle u_z^{(2)}(\rho) \rangle = G_3. \quad (\text{B28c})$$

The second-order pressure has the form $p^{(2)} = p^{(20)}(\rho) + p^{(21)}(\rho) \sin[2(m\phi + z - t)]$, and therefore its time average is also independent of ϕ and z . Then the second-order terms of all the components of $\boldsymbol{\tau}$ and \mathbf{F} vanish, except that of τ_z which turns out to be proportional to H_1 . So the

zero-torque condition is enforced by setting H_1 to 0. Evaluating E_1 , H_2 , and G_3 using Eq. (D4) and inserting them back into Eqs. (B28):

$$\langle u_\rho^{(2)} \rangle = 0, \quad (\text{B29a})$$

$$\langle u_\phi^{(2)} \rangle = -\rho \frac{[a_s K_{m-1}(a_s) + m K_m(a_s)] \mathcal{G}_m(a_s)}{2 \mathcal{F}_m(a_s) [1 + (m/a_s)^2]}, \quad (\text{B29b})$$

$$\langle u_z^{(2)} \rangle = \frac{m[(2-m)K_m(a_s) - a_s K_{m-1}(a_s)] \mathcal{G}_m(a_s)}{2a_s^2 \mathcal{F}_m(a_s) [1 + (m/a_s)^2]}, \quad (\text{B29c})$$

where

$$\mathcal{G}_m(a_s) = a_s [K_{m-1}(a_s)^2 - K_m(a_s)^2] + 2m K_m(a_s) K_{m-1}(a_s). \quad (\text{B30})$$

Again, one should multiply the above expressions with ω/k_z to obtain the value of $\langle \mathbf{u}^{(2)} \rangle$ in the original units.

APPENDIX C: CALCULATION OF $\mathcal{W}^{(0)}$

The work performed by the cylinder on the fluid (in the units used in the main text):

$$\mathcal{W} = -\frac{k_z}{2\pi(2\pi a)} \int \mathbf{u} \cdot \boldsymbol{\sigma}_s \cdot d\mathbf{A} = -\frac{k_z}{2\pi(2\pi a)} \int_0^{2\pi} \int_{-\pi/k_z}^{\pi/k_z} \mathbf{u} \cdot \boldsymbol{\sigma}_s \cdot \hat{\mathbf{n}} \text{Det}[\mathbf{g}]^{1/2} d\phi dz. \quad (\text{C1})$$

The leading-order term of \mathcal{W} reads

$$\mathcal{W}^{(0)} = -\frac{k_z}{2\pi(2\pi a)} \epsilon^2 \int_0^{2\pi} \int_{-\pi/k_z}^{\pi/k_z} [\mathbf{u}^{(1)} \cdot \boldsymbol{\sigma}^{(1)} \cdot \hat{\boldsymbol{\rho}}]_a a d\phi dz, \quad (\text{C2})$$

where

$$\epsilon \boldsymbol{\sigma}^{(1)} = \epsilon [\eta (\nabla \mathbf{u}^{(1)} + \nabla \mathbf{u}^{(1)T}) - p^{(1)}] \quad (\text{C3})$$

is the first-order term of the stress tensor given by Eq. (2). Then, from the boundary condition (9),

$$\mathcal{W}^{(0)} \simeq \frac{ck_z}{(2\pi)^2} \epsilon^2 \int_0^{2\pi} \int_{-\pi/k_z}^{\pi/k_z} \sigma_{\rho\rho}^{(1)}(\rho = a) \cos(m\phi + k_z z - \omega t) d\phi dz,$$

and using Eqs. (11) and $p^{(1)} = p^{(10)}(\rho) \cos(m\phi + k_z z - \omega t)$, we find

$$\mathcal{W}^{(0)} = \frac{c\epsilon^2}{2} \left[2\eta \frac{du_\rho^{(10)}}{d\rho} - p^{(10)} \right]_a. \quad (\text{C4})$$

Substituting (B18a) and (B22) into the above equation:

$$\begin{aligned} \mathcal{W}^{(0)} = \eta \epsilon^2 c \omega \left[\frac{(24m^2 - 3ma_s^2 + 32m - 16a_s^2) K_{m+1}(a_s) K_m(a_s)^2 + a_s (-28m + a_s^2 - 16) K_{m+1}(a_s)^2 K_m(a_s)}{8a_s \mathcal{F}_m(a_s) [1 + (m/a_s)^2]} \right. \\ \left. + \frac{K_{m-1}(a_s) [(4m - a_s^2) K_{m+1}(a_s) + ma_s K_m(a_s)] K_m(a_s) + 8a_s K_{m+1}(a_s)^3 + 2m(m+8) K_m(a_s)^3}{8\mathcal{F}_m(a_s) [1 + (m/a_s)^2]} \right]. \quad (\text{C5}) \end{aligned}$$

APPENDIX D: THE ($m = 1, k_z = 0$) CASE

Here we present the calculation for $m = 1$ and $k_z = 0$. In this case, the radial coordinate of a surface point at (ϕ, z) is given by $R(\phi, t) = a + b \sin(\phi - \omega t)$. We assume that $b \ll a$. Again, we solve Eq. (B2) in a cylindrical coordinate system attached to the cylinder. The no-slip boundary condition at the surface of the cylinder leads to

$$\mathbf{u}(\rho = R, \phi, z) = \frac{dR}{dt} \hat{\boldsymbol{\rho}} = -b\omega \cos(\phi - \omega t) \hat{\boldsymbol{\rho}}. \quad (\text{D1})$$

As we assume that $b \ll a$, expanding \mathbf{u} and p in $\epsilon \equiv b/a$:

$$\mathbf{u} = \epsilon \mathbf{u}^{(1)} + \epsilon^2 \mathbf{u}^{(2)} + \dots, \quad (\text{D2a})$$

$$p = \epsilon p^{(1)} + \epsilon^2 p^{(2)} + \dots. \quad (\text{D2b})$$

Then the leading-order terms of Eq. (D1) give

$$\mathbf{u}^{(1)}(\rho = a) = -\omega a \cos(\phi - \omega t) \hat{\boldsymbol{\rho}}, \quad (\text{D3})$$

$$\mathbf{u}^{(2)}(\rho = a) = -a \left. \frac{\partial \mathbf{u}^{(1)}}{\partial \rho} \right|_a \sin(\phi - \omega t). \quad (\text{D4})$$

Here the velocity field does not depend on z , so the incompressibility condition, $\nabla \cdot \mathbf{u} = 0$, suggests that the $\mathbf{u}^{(1)}$ can be written as the curl of a stream function $\hat{\mathbf{z}}\Psi^{(1)}(\rho, \phi)$:

$$\mathbf{u}^{(1)} = \nabla \times [\Psi^{(1)}(\rho, \phi) \hat{\mathbf{z}}]. \quad (\text{D5})$$

Then Eq. (B2) reduces to

$$\nabla^4 \Psi^{(1)} = 0. \quad (\text{D6})$$

The boundary condition (D3) hints that the solution of the above equation has the following form:

$$\Psi^{(1)}(\rho, \phi) = \Psi_0^{(1)}(\rho) \cos(\phi - \omega t). \quad (\text{D7})$$

Substituting the above into Eq. (D6) and solving the resulting equation for $\Psi_0^{(1)}$ yields

$$\Psi_0^{(1)}(\rho) = L_4 \rho^3 + L_2 \rho + \frac{L_1}{\rho} + L_3 \ln(\rho). \quad (\text{D8})$$

The components of $\mathbf{u}^{(1)}$ are then given by

$$u_\rho^{(1)} = \left(3L_4 \rho^2 - \frac{L_1}{\rho^2} + L_3 \ln(\rho) + L_2 + L_3 \right) \cos(\phi - \omega t),$$

$$u_\phi^{(1)} = -\left(L_4 \rho^2 + L_2 + L_3 \ln(\rho) + \frac{L_1}{\rho^2} \right) \sin(\phi - \omega t),$$

$$u_z^{(1)} = 0.$$

To avoid the diverging behavior of velocity field at $\rho \rightarrow \infty$, we set L_4 and L_3 to zero. That gives

$$u_\rho^{(1)} = \left(-\frac{L_1}{\rho^2} + L_2 \right) \cos(\phi - \omega t), \quad (\text{D9})$$

$$u_\phi^{(1)} = -\left(L_2 + \frac{L_1}{\rho^2} \right) \sin(\phi - \omega t), \quad (\text{D10})$$

$$u_z^{(1)} = 0. \quad (\text{D11})$$

Using the boundary condition (D3), we find that $L_1 = a^3 \omega / 2$ and $L_2 = -a \omega / 2$. So the final expressions of the components of $\mathbf{u}^{(1)}$ are

$$u_\rho^{(1)} = -\frac{a\omega}{2} \left(\frac{a^2}{\rho^2} + 1 \right) \cos(\phi - \omega t), \quad (\text{D12})$$

$$u_\phi^{(1)} = -\frac{a\omega}{2} \left(\frac{a^2}{\rho^2} - 1 \right) \sin(\phi - \omega t), \quad (\text{D13})$$

$$u_z^{(1)} = 0. \quad (\text{D14})$$

Therefore, in the laboratory frame, the leading-order velocity field at $\rho \rightarrow \infty$ will be

$$-\lim_{\rho \rightarrow \infty} \mathbf{u}^{(1)} \epsilon = \frac{b\omega}{2} \cos(\phi - \omega t) \hat{\rho} - \frac{b\omega}{2} \sin(\phi - \omega t) \hat{\phi} = \frac{b\omega}{2} \cos(\omega t) \hat{\mathbf{x}} + \frac{b\omega}{2} \sin(\omega t) \hat{\mathbf{y}}. \quad (\text{D15})$$

-
- [1] E. Lauga and T. R. Powers, The hydrodynamics of swimming microorganisms, *Rep. Prog. Phys.* **72**, 096601 (2009).
 - [2] G. Taylor, Analysis of the swimming of microscopic organisms, *Proc. R. Soc. London A* **209**, 447 (1951).
 - [3] G. I. Taylor, The action of waving cylindrical tails in propelling microscopic organisms, *Proc. R. Soc. London A* **211**, 225 (1952).
 - [4] M. J. Lighthill, On the squirming motion of nearly spherical deformable bodies through liquids at very small Reynolds numbers, *Commun. Pure Appl. Math.* **5**, 109 (1952).
 - [5] J. Blake, Self propulsion due to oscillations on the surface of a cylinder at low Reynolds number, *Bull. Austral. Math. Soc.* **5**, 255 (1971).
 - [6] J. R. Blake, A spherical envelope approach to ciliary propulsion, *J. Fluid Mech.* **46**, 199 (1971).
 - [7] T. Ishikawa, M. P. Simmonds, and T. J. Pedley, Hydrodynamic interaction of two swimming model microorganisms, *J. Fluid Mech.* **568**, 119 (2006).
 - [8] T. Ishikawa, G. Sekiya, Y. Imai, and T. Yamaguchi, Hydrodynamic interactions between two swimming bacteria, *Biophys. J.* **93**, 2217 (2007).
 - [9] M. Farzin, K. Ronasi, and A. Najafi, General aspects of hydrodynamic interactions between three-sphere low-Reynolds-number swimmers, *Phys. Rev. E* **85**, 061914 (2012).
 - [10] A. Reynolds, The swimming of minute organisms, *J. Fluid Mech.* **23**, 241 (1965).
 - [11] D. F. Katz, On the propulsion of micro-organisms near solid boundaries, *J. Fluid Mech.* **64**, 33 (1974).
 - [12] D. G. Crowdy and Y. Or, Two-dimensional point singularity model of a low-Reynolds-number swimmer near a wall, *Phys. Rev. E* **81**, 036313 (2010).
 - [13] S. E. Spagnolie and E. Lauga, Hydrodynamics of self-propulsion near a boundary: Predictions and accuracy of far-field approximations, *J. Fluid Mech.* **700**, 105 (2012).
 - [14] J. Dunstan, G. Miño, E. Clement, and R. Soto, A two-sphere model for bacteria swimming near solid surfaces, *Phys. Fluids* **24**, 011901 (2012).
 - [15] E. Lauga, Propulsion in a viscoelastic fluid, *Phys. Fluids* **19**, 083104 (2007).
 - [16] J. Teran, L. Fauci, and M. Shelley, Viscoelastic Fluid Response Can Increase the Speed and Efficiency of a Free Swimmer, *Phys. Rev. Lett.* **104**, 038101 (2010).
 - [17] X. N. Shen and P. E. Arratia, Undulatory Swimming in Viscoelastic Fluids, *Phys. Rev. Lett.* **106**, 208101 (2011).
 - [18] J. R. Vélez-Cordero and E. Lauga, Waving transport and propulsion in a generalized Newtonian fluid, *J. Non-Newtonian Fluid Mech.* **199**, 37 (2013).
 - [19] C. Datt, L. Zhu, G. J. Elfring, and O. S. Pak, Squirming through shear-thinning fluids, *J. Fluid Mech.* **784**, R1 (2015).
 - [20] M. S. Krieger, S. E. Spagnolie, and T. R. Powers, Locomotion and transport in a hexatic liquid crystal, *Phys. Rev. E* **90**, 052503 (2014).
 - [21] J. Shi and T. R. Powers, Swimming in an anisotropic fluid: How speed depends on alignment angle, *Phys. Rev. Fluids* **2**, 123102 (2017).
 - [22] H. Soni, R. A. Pelcovits, and T. R. Powers, Enhancement of Microorganism Swimming Speed in Active Matter, *Phys. Rev. Lett.* **121**, 178002 (2018).
 - [23] M. S. Krieger, S. E. Spagnolie, and T. R. Powers, Swimming with small and large amplitude waves in a confined liquid crystal, *J. Non-Newtonian Fluid Mech.* **273**, 104185 (2019).
 - [24] N. C. Darnton, L. Turner, S. Rojevsky, and H. C. Berg, On torque and tumbling in swimming *Escherichia coli*, *J. Bacteriol.* **189**, 1756 (2007).

- [25] J. de Anda, E. Y. Lee, C. K. Lee, R. R. Bennett, X. Ji, S. Soltani, M. C. Harrison, A. E. Baker, Y. Luo, T. Chou *et al.*, High-speed “4D” computational microscopy of bacterial surface motility, *ACS Nano* **11**, 9340 (2017).
- [26] C. N. Dominick and X.-L. Wu, Rotating bacteria on solid surfaces without tethering, *Biophys. J.* **115**, 588 (2018).
- [27] L. Kužicki, T. L. Jahn, and J. R. Fonesca, Helical nature of the ciliary beat of paramecium multimicronucleatum, *J. Protozool.* **17**, 16 (1970).
- [28] S. E. Spagnolie, B. Liu, and T. R. Powers, Locomotion of Helical Bodies in Viscoelastic Fluids: Enhanced Swimming at Large Helical Amplitudes, *Phys. Rev. Lett.* **111**, 068101 (2013).
- [29] B. Liu, T. R. Powers, and K. S. Breuer, Force-free swimming of a model helical flagellum in viscoelastic fluids, *Proc. Natl. Acad. Sci. USA* **108**, 19516 (2011).
- [30] L. D. Landau and E. M. Lifshitz, *Fluid Mechanics, Course of Theoretical Physics*, Vol. 6 (Elsevier, 2013).
- [31] G. K. Batchelor, Slender-body theory for particles of arbitrary cross-section in Stokes flow, *J. Fluid Mech.* **44**, 419 (1970).
- [32] J.-L. Pierson, M. Kharrouba, and J. Magnaudet, Hydrodynamic torque on a slender cylinder rotating perpendicularly to its symmetry axis, *Phys. Rev. Fluids* **6**, 094303 (2021).
- [33] J. R. Blake and M. A. Sleight, Mechanics of ciliary locomotion, *Biol. Rev.* **49**, 85 (1974).
- [34] H. Machemer, Ciliary activity and the origin of metachrony in *Paramecium*: Effects of increased viscosity, *J. Exp. Biol.* **57**, 239 (1972).
- [35] S. L. Tamm, Ciliary motion in *Paramecium*: A scanning electron microscope study, *J. Cell Biol.* **55**, 250 (1972).